Available online at www.sciencedirect.com
SCIENCE DIRECT®
Corrosion Science 46 (2004) 1431–1465
CORROSION SCIENCE
www.elsevier.com/locate/corsci

Advances in understanding atmospheric corrosion of iron. II. Mechanistic modelling of wet–dry cycles

S. Hœrlé [a], F. Mazaudier [a], Ph. Dillmann [b,*], G. Santarini [c]

[a] *Laboratoire d'Etude de la Corrosion Aqueuse DEN/DPC/SCCME, CEA Saclay, 91191 Gif Sur Yvette, France*
[b] *Laboratoire Pierre Süe, CEA/CNRS, DRECAM/DSM, CEA Saclay, 91191 Gif Sur Yvette cedex, France*
[c] *Service de la Corrosion et du Comportement des Matériaux dans leur Environnement, DEN/DPC, CEA Saclay, 91191 Gif Sur Yvette, France*

Received 14 January 2003; accepted 18 September 2003

Abstract

With the aim of predicting the long term atmospheric corrosion behaviour of iron, the mechanisms occurring inside the rust layer during a wet–dry cycle are considered as well as the characteristics of the rust layer formed during this process. A first step in modelling the behaviour is proposed, based on the description of the cathodic reactions associated with iron oxidation: reduction of a part of the rust layer (lepidocrocite) and reduction of dissolved oxygen on the rust layer. The blocking of the anodic sites is considered to describe the extinction of electrochemical corrosion during the drying. The modelling, by including some composition and morphological data of the rust layer as parameters is able to account for the metal damage after one wet–dry cycle.
© 2003 Elsevier Ltd. All rights reserved.

Keywords: C. Atmospheric corrosion; C. Rust; A. Iron; B. Modelling studies

1. Introduction

Nuclear waste could be packaged in metallic containers and disposed in very long term interim dry storages for about 100 years. Nevertheless, in such conditions

* Corresponding author. Tel.: +33-1-69-08-14-69; fax: +33-1-69-08-69-23.
E-mail address: philippe.dillmann@cea.fr (Ph. Dillmann).

0010-938X/$ - see front matter © 2003 Elsevier Ltd. All rights reserved.
doi:10.1016/j.corsci.2003.09.028

(environmental corrosion), condensation on the metallic containers, due to ambient temperature and humidity fluctuations, cannot be completely prevented (e.g. thermal powerless containers). The containers walls may then be exposed to cyclic wet and dry periods and will suffer from indoor atmospheric corrosion at room temperature.

The atmospheric corrosion behaviour of iron based materials such as carbon or low alloy steels has generally been well predicted for periods of a few tens of years by the well-known bilogarithmic laws [1,2]. For longer time periods of one to a few centuries, which could be the case for some nuclear waste containers in very long term storage, predictions are rare and probably more uncertain. The main reason of this lack of reliability is the complex mechanisms involving the rust layer during atmospheric corrosion cycles and the subsequent modifications of the protective properties of the rust scale. A mechanistic modelling of these phenomena appears then to be necessary to establish more relevant and robust prediction of corrosion allowance in the behaviour of materials such as iron or low alloy steels. The aim being long term prediction of the containers damage, predictive equations of such a damage are required.

Basic considerations on atmospheric corrosion and the involved electrochemical phenomena are presented in Section 2, before to examine in more detail the studied system in Section 3. The modelling of the different stages of atmospheric corrosion is presented in Section 4 and discussed in Section 5.

2. Atmospheric corrosion—literature survey

In this section, general considerations about atmospheric corrosion (AC) are presented, along with a literature survey of the involved mechanisms that are of some use for the modelling.

2.1. Atmospheric corrosion

Contrary to dry oxidation, AC is, by nature, an electrochemical process needing aqueous conditions for its occurrence. As far as iron or low alloy steels are concerned, AC can be summarised by the stoichiometric equilibrium [3]:

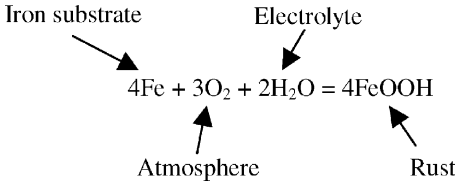

(I)

From Eq. (I), one can extract the main features of AC: oxidation of iron by an atmospheric oxidiser (O_2), under a water layer (electrolyte) that leads to the formation of a rust layer. Through its electronic conduction and mass transport properties the rust layer has a feedback effect on AC mechanisms. One has to keep in mind that the rust layer is actually far more complex than suggested by Eq. (I). It is

Table 1
Some of the oxides and hydroxides found in rust layers

Composition	Name	Crystal system
Fe_3O_4	Magnetite*	Cubic (spinel)
γ-Fe_2O_3	Maghemite	Cubic (spinel)
α-FeOOH	Goethite*	Orthorhombic
γ-FeOOH	Lepidocrocite*	Orthorhombic
β-FeOOH	Akaganeite	Tetragonal
γ-Fe·OH·OH	Reduced lepidocrocite	Orthorhombic
$Fe(OH)_2$	Ferrous hydroxide	Hexagonal

A $*$ indicates the most common species. The reduced lepidocrocite is an hypothetical phase as discussed in Section 2.3.

composed of several oxides and hydroxides as presented in Table 1. A more detailed description of the rust layer is given in Section 3.

Interactions between the electrolyte and the rust layer are the key features of AC and are examined in the following sub-sections.

2.2. Electrolyte formation

An aqueous layer, which acts as an electrolyte, is formed in indoor conditions by water condensation. The time of wetness, which defines the duration of the electrochemical process, is strongly dependent on many parameters which include the water vapour content of the atmosphere, i.e. the relative humidity (RH) at a given temperature. It is generally considered that AC of carbon or weathering steels begins at about 60% RH with a very slow rate and increases sharply at $80\% \leqslant RH < 100\%$ [4]. When a 100% RH is reached, a $\sim$100 μm electrolyte thickness can be observed.

The RH and temperature variations lead to cyclic wet and dry periods, the so-called wet–dry cycles (Fig. 4).

The wet–dry cycles are a critical feature of AC as the alternating wet and dry periods drastically change the rusting mechanisms from those obtaining in bulk aqueous corrosion. Indeed, earlier studies have shown that during a wet–dry cycle, the AC of iron or low alloy steel can be divided into three stages. As initially proposed by Evans and Taylor [5] and then experimentally investigated by Stratmann et al. [6,7], during the first stage (wetting), the anodic dissolution of iron is mainly balanced by the reduction of ferric species within the rust layer and very little oxygen is reduced. After the reducible species are used up, the second stage (wet stage) begins, characterised by oxygen reduction as the major cathodic reaction. Eventually, at the end of the drying, the third stage of the cycle, the species reduced during the first stage and other ferrous compounds produced by the corrosion processes are re-oxidised by oxygen. Finally, the electrolyte film evaporates, thus dramatically slowing down the electrochemical corrosion. The corrosion rate and the rust layer modifications are thus correlated to the number and frequency of the wet–dry cycles.

The different stages of AC are examined in further detail in the following.

2.3. Wetting stage

During the wetting, i.e. in the electrolyte build up, the anodic dissolution of iron begins. The electrons produced by this oxidation have to be consumed by a reduction reaction. Dissolved oxygen is obviously available as an oxidiser. Nevertheless, oxygen cannot be reduced on the rust layer, as it is not conducting (see Section 3). Furthermore, the metal surface left in contact with electrolyte by the rust layer is, in one hand, very small and, in other hand, difficult of access by oxygen, which has to diffuse through the thick rust layer (~100 μm) via tortuous pores of nanometric width. So oxygen reduction cannot provide the large corrosion rates observed during the wetting stage [6]. Another available oxidiser is γ-FeOOH, present in the rust layer. One of the proposed reduction reactions [5,8–10] for γ-FeOOH is

$$\gamma\text{-FeOOH} + e^- + H^+ \rightarrow \gamma\text{-Fe}\cdot\text{OH}\cdot\text{OH} \quad \text{(II)}$$

According to Stratmann et al. [8,9], the reduced lepidocrocite (γ-Fe·OH·OH) would be a compound of same chemical formula as iron hydroxide but keeping the same crystallographic structure as its mother phase γ-FeOOH. It would be a Fe^{2+} doped lepidocrocite: Fe[II] being in Fe sites and OH^- being in O sites. The reduced lepidocrocite would keep the same crystallographic structure as γ-FeOOH as long as the Fe^{2+} doping concentration in the lattice is less than 2–4% [8], at which point Fe_3O_4 begins to form irreversibly. γ-Fe·OH·OH becomes back lepidocrocite when the rust layer is oxidised, whereas magnetite is stable or slightly oxidised into maghemite (γ-Fe_2O_3).

The Fe^{2+} doping turns the reduced lepidocrocite into an electronic conductor and its crystallographic structure would allow ionic conduction [8,11].

Reaction (II) requires electrons, it starts then at the metal/rust interface and the reduction front spreads through the rust layer as γ-Fe·OH·OH is an electronic conductor. The conductive properties of the rust layer change then with the progression of the reduction front.

It was experimentally observed that the reduction of γ-FeOOH is limited to a few monolayers of γ-FeOOH crystals on the surface of the pores [8,12].

Reduced lepidocrocite γ-Fe·OH·OH was not experimentally observed, but the fast and reversible reduction of γ-FeOOH suggests a solid state transformation rather than a dissolution–precipitation mechanism [9]. Moreover, Mössbauer analyses show that in the formed compound, iron is more firmly bound to the lattice than in the case of a more gel-like precipitated iron hydroxide [9,13].

The reduction reaction goes on all over the γ-FeOOH reducible surface and reduced γ-FeOOH finally coats the rust layer (Fig. 1). This depends on the porosity of the rust layer, the surface of the pores and the amount of γ-FeOOH on this surface. It should be pointed out here that the fraction of lepidocrocite in the rust layer and thus the γ-FeOOH amount on the surface of the pores (which is described by α/γ, the α-FeOOH and γ-FeOOH composition ratio, when the rust layer is considered to be formed only of these compounds, see Section 3) characterises the ability of the rust layer to be reduced, and then, conversely, its protective ability.

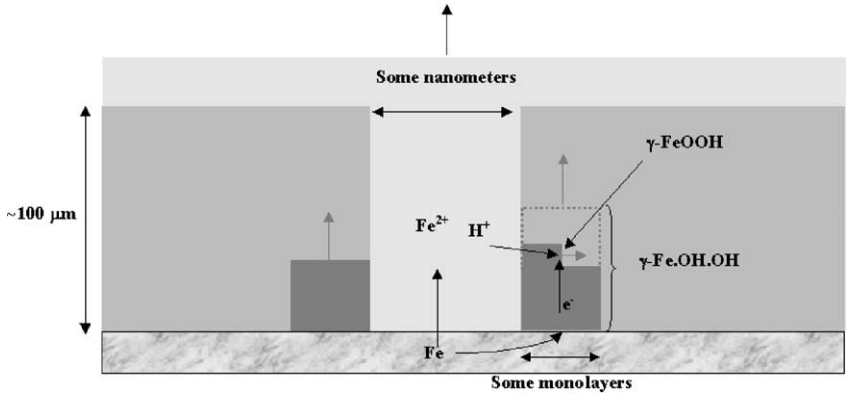

Fig. 1. Schematic representation of the phenomena occurring during the wetting.

Basing on experimental results showing that the amount of reduced lepidocrocite depends on the applied potential, Kuch [14] has developed a modelling of lepidocrocite reduction controlled by electron transfer and that can be described by a Butler–Volmer law. The reduction reaction is

$$3\gamma\text{-FeOOH} + H^+ + e^- \rightarrow Fe_3O_4 + 2H_2O \qquad \text{(III)}$$

In this description, there are two compounds of different crystallographic structures (γ-FeOOH and Fe_3O_4). It appears to us more suitable to consider reaction (II), where the reduced compound (γ-Fe·OH·OH), keeps the same crystallographic structure as the mother phase. It is then possible to consider the formation of a solid solution γ-FeOOH/γ-Fe·OH·OH. This will be used in our modelling.

During the wetting stage, it is the rust layer itself that is responsible for corrosion, the anodic dissolution being balanced by the reduction of γ-FeOOH within the rust layer.

2.4. Wet stage

When a large part of the available γ-FeOOH is reduced to the conducting γ-Fe·OH·OH, it coats the surface developed by the rust layer porosity. If a connection between the underlying metal exists then the reduced γ-Fe·OH·OH on the surface of the pores can act as a cathodic area. Oxygen can then be reduced on that surface. Cathodic and anodic areas are decoupled, the oxidation of iron taking place on the small metal area in contact with electrolyte at the bottom of the pores and the reduction reaction on the large cathodic area formed by the reduced γ-FeOOH (Fig. 2).

The oxygen reduction current behaviour differs during the wet–dry cycle: During the wet stage it is almost constant (Fig. 4) but at the end of the wet stage, the oxygen reduction current increases (and then decreases during the beginning of the drying, see following Section 2.5).

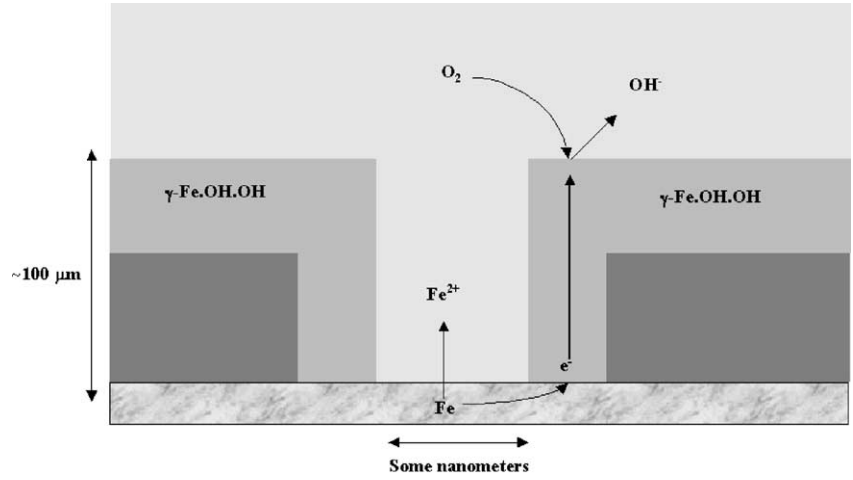

Fig. 2. Schematic representation of the phenomena occurring during the wet stage.

The increase of the oxygen reduction current is explained by the decrease of the diffusion path. Many authors have observed a current variation inversely proportional to the electrolyte thickness when it is decreased [10,15–18]. This behaviour is observed as long as the electrolyte thickness is greater than about 10 μm. Moreover, the potential increases as the electrolyte thickness decreases. This potential increase is measured only in the presence of oxygen [18].

On platinum electrode, the oxygen reduction current becomes constant when the electrolyte film is very thin (about 10 μm) whereas it dramatically decreases on iron electrode [17]. The decrease of oxygen reduction current is then attributed to the blocking of the dissolution sites by the corrosion products (see following Section 2.5).

These experimental evidences support a diffusion control of the oxygen reduction, at least as long as the electrolyte layer is enough thick (>10 μm). Furthermore, the behaviour of the oxygen reduction current with electrolyte thickness suggests also that the oxygen reduction takes place, if not completely, at least in a large part, on the outer surface of the rust layer (that also provides a larger cathodic area than the metal [7]). Indeed, if the diffusion path was through the rust layer there would not be such an electrolyte thickness dependence of the reduction current.

However, the literature measurements were done on relatively fresh rust layers and not on old and thick (>100 μm) ones as expected for long term AC corrosion. In the case of old rust layers, it is far from sure that all the rust layer could be reduced during the wetting stage and no experimental results on the variation of oxygen reduction current with electrolyte thickness are available in this case. It is then difficult to conclude on oxygen reduction in old rust layers.

For the modelling, it will be considered that oxygen reduction occurs inside the rust layer (oxygen has then to enter into the pores to be reduced) and that the reduction reaction is under mixed diffusion and transfer control.

The actual mechanism of oxygen reduction is somewhat complicated and has not yet been clearly resolved in the presence of iron oxides [19]. Different mechanisms were proposed that differ by adsorption steps and number of electrons exchanged (2–4) during the rate determining step. The common point between the mechanisms is the formation of a catalytic intermediate, H_2O_2, for instance following heterogeneous catalytic electrode reaction (HCER) scheme [20–22]:

$$O_2 + 2H_2O + 2e^- = H_2O_{2,S} + 2OH^- \quad \text{(IV)}$$

$$H_2O_{2,S} \rightarrow \tfrac{1}{2}O_2 + H_2O \quad \text{(V)}$$

The real mechanism depends particularly on the potential as well as the nature of the oxide or hydroxide on which the reduction reaction takes place. The Fe^{2+} states catalyse the decomposition of H_2O_2. The reduction rate is then accelerated on magnetite or lepidocrocite doped with Fe^{2+} by its own reduction.

Because of the large variety of proposed mechanisms, often depending on particular cases, for purposes of modelling only the overall reduction reaction is considered:

$$O_2 + 4e^- + 2H_2O \xrightarrow{k} 4OH^- \quad \text{(VI)}$$

2.5. Drying stage

During the drying, the electrolyte thickness decreases. When it becomes thinner than a threshold of about 10 μm, a drop in the reduction current is observed. Several phenomena are proposed to explain this decrease. First, on pure iron, it is observed that when the electrolyte thickness is very thin, the reduction current becomes constant. It seems that it is then no more oxygen diffusion, but oxygen solvation that determines the reduction rate [17]. This explains the independence of the current from the electrolyte thickness, not its decrease.

Another explaining is simply that the drying reduces the anodic and cathodic areas and then "switch down" the electrochemical reactions by the lack of electrolyte [15].

Some authors, suggest mechanisms linked to passivation. The decrease of the electrolyte thickness comes with an increase of the concentration of the species dissolved during the first stages of the wet–dry cycle. These species reach their precipitation limits and coat the surface. Although it decreases both cathodic and anodic areas, it is the small anodic area that is mainly affected and iron dissolution is then prevented.

The anodic current is then limited by the blocking of the anodic sites and also by the diffusion of the dissolved species because of the increase of their concentrations due to the decrease of the electrolyte thickness.

More, the "electron pumping" of the cathodic reaction, enhanced by the electrolyte thickness decrease, shifts the potential toward more anodic values [23,24]. Some authors evoke then genuine passivation [18], when the potential becomes more anodic, helped by a more alkaline pH, due to oxygen reduction.

The oxidation current becomes then weaker, and the system turns into anodic control.

All these mechanisms are certainly involved, more or less, at different steps of the drying. For the modelling, we will narrow to passivation-like phenomena due to the potential increase and the blocking of the anodic sites, that turn the system from a cathodic control into an anodic one.

At the end of the drying, the increasing of cathodic current polarises the rust layer to more positive potentials, allowing oxidation of ferrous species. The γ-FeOOH species is regenerated from γ-Fe·OH·OH by the reverse (II) reaction, thus allowing another cycle to occur when the rust is wetted again [8]. Some α-FeOOH may also be formed from $Fe(OH)_2$ precipitates, which increases the protective ability of the rust, cycle after cycle. Moreover, by diminishing the amount of surface γ-Fe·OH·OH sites, the oxidation process also decreases the cathodic area, which lessens the current (Fig. 3).

To sum up, there is an activity peak during the drying. First, the corrosion rate is increased by the diminution of the dissolved oxygen diffusion path, and then it is decreased both by blocking of the anodic sites and re-oxidation of conducting γ-Fe·OH·OH into insulating γ-FeOOH.

During the last instant of the drying stage, there is quite no more corrosion, but modifications of the rust layer composition and structure can occur that may dramatically change its protective properties and this can be critical for long term behaviour.

What appears to us the main features of the mechanisms involved in AC wet–dry cycles that have to be modelled are electrochemical phenomena associated with each stage: γ-FeOOH reduction during the wetting, oxygen reduction during the wet stage and blocking of the anodic sites during the drying.

As it may emerge from this brief description of the mechanisms and literature survey, the system rust layer + electrolyte + wet–dry cycle is rather complex and requires then drastic simplifications for the modelling.

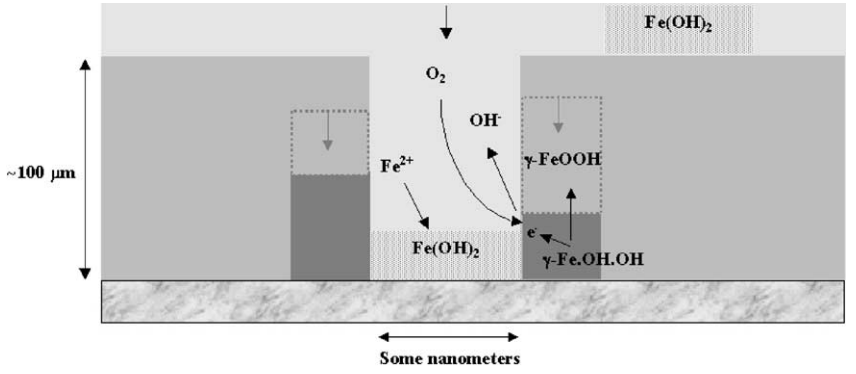

Fig. 3. Schematic representation of the phenomena occurring during drying.

3. System study and simplification

In this section, the main components of the system (electrolyte, wet–dry cycle and rust layer) and their simplified models are presented.

3.1. Electrolyte

As it is detailed in rust layer sub-section, rust layers are porous and heterogeneous media. The electrolyte build up during the wetting (and its evaporation during the drying) is then very complex. Water condensation inside the pores depends on the pores structure (e.g. pore diameters) and it is likely that some nanometric scale pores are never wholly dried [25].

To make it easier for the modelling, the electrolyte is assumed to be a layer of constant thickness d over all the surface of the rust layer. It is assumed that the rust layer is "instantly" wetted and that the electrolyte film thickness grows until reaching a stationary value for the wet stage. And reciprocally for the drying. The wetting and drying mechanisms of the pores are then not considered. This is called the "macroscopic" electrolyte film model: An electrolyte film which thickness increases and decreases during the wet–dry cycle from the rust layer outer surface to a stationary value (Figs. 4 and 6b).

As the atmosphere is assumed to be only pure air with water vapour, the electrolyte film is made of only water with dissolved oxygen.

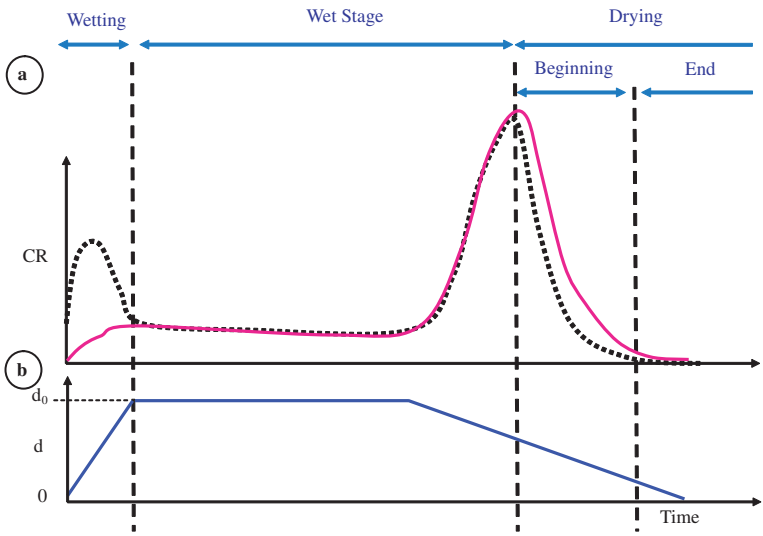

Fig. 4. (a) Sketch of the wet–dry cycle (from Stratmann [23]) and the different stages used for the modelling (variations of iron (dotted line) and oxygen (solid line) consumption rates (CR)). (b) The schematic variations of electrolyte thickness (d) in the "macroscopic" electrolyte model.

3.2. Wet–dry cycles

Whereas all the parameters are highly correlated and the phenomena described in Section 2 may, during intermediate stages, occur simultaneously, a typical wet–dry cycle will be considered for the modelling. This cycle is composed of a wetting stage with only γ-FeOOH reduction, a wet stage when only oxygen is reduced (including then a part of the actual drying) and a drying stage, more complex, that corresponds to the competition between increased oxygen reduction rate and precipitation/passivation leading to the extinction of corrosion processes.

For purposes of modelling, the wet–dry cycle as presented in the previous section, is cut out as follows (Fig. 4):

Variation of electrolyte thickness

- *Wetting*. Electrolyte thickness increases from the surface of the rust layer, to the stationary value $d = d_0$.
- *Wet stage*. $d = d_0$.
- *Drying*: d decreases from d_0 to 0 (surface of the rust layer).

The wetting and drying mechanisms of the pore network are not considered (or assumed to be instantaneous).

Mechanisms

- *Wetting*. The cathodic reaction is γ-FeOOH reduction, the system is under *cathodic control*.
- *Wet stage*. The cathodic reaction is O_2 reduction, the system is under *cathodic control*.
- *Beginning of the drying*. The cathodic reaction is O_2 reduction, anodic sites are being blocked, the system is under *anodic control*.
- *End of the drying*. There is quite no more electrochemical corrosion. The rust layer is re-oxidised.

The different stages are assumed to be independent from each other and will be modelled separately.

3.3. Rust layer

As shown by the description of the wet–dry cycles, it is mainly the rust layer that is involved in the electrochemical phenomena and so determines the transport processes that are indispensable for corrosion to occur. The composition and structure of the rust layer are then of some importance for the development of AC. A more detailed description of the rust layer and a presentation of the techniques used for its characterisation are presented elsewhere [26,27].

A real rust layer is a very complex object (Fig. 6a). It is mainly composed of iron oxy-hydroxides and some other oxides such as lepidocrocite (γ-FeOOH), goethite (α-FeOOH) and magnetite (Fe_3O_4), to mention only the most common. The relative

fraction of these compounds is an important factor in determining the protective ability of the rust layer. Lepidocrocite γ-FeOOH is a semi-conducting and electrochemically active species [28], α-FeOOH is insulating and non-active [29,30] and Fe_3O_4, although a good conductor is considered as protective because of its compactness and thermodynamic stability [28,29].

For purposes of simplicity, a rust layer composed of only two species, a protective (say α-FeOOH) and an active (say γ-FeOOH) will be considered for the modelling. The composition of the rust layer and, to a certain extent, its protective ability, are characterised by the α-FeOOH and γ-FeOOH composition ratio α/γ, which we call the protective ability index. For ancient rusts, the protective ability index ranges from about 1 to 5 [26,27]. For the modelling, it is not the protective ability index that is used, but the fraction of lepidocrocite:

$$\beta = \frac{\gamma}{\alpha + \gamma} = \frac{1}{1 + \frac{\alpha}{\gamma}}. \tag{1}$$

Obviously, in the rust layer, there are also some species coming either from the external atmosphere (e.g. dust particles incorporated during the rust growth or sulphur compounds coming from industrial fumes) or from the underlying metal, alloying elements or slag inclusions (Cu, P, Cr, ...). To begin with, they will not be considered, although they may have dramatic impacts on rusting [4,5,31–35]. The modelling will then be restricted to AC of pure iron in an atmosphere free from any pollutant. The protective ability of the rust layer is also determined by its structural properties. Indeed, the corrosion processes are governed by mass transport through the rust layer and by the surface of the pores. Given the mean thickness of a few 10-year-old rust layer (~100 μm), it would seem that the transport phenomena probably depend mainly on diffusion and migration in the electrolyte through the pore network of the rust. The measured porosity of old rust layers, whatever their composition and structure is a few percent (~10%) [26,27] with mainly tortuous pores of nanometric width. These old rust layers are quite protective as a result of their compactness, which is not perhaps the case with fresh rust layers that are far more likely to be porous.

When active species, as dissolved oxygen, have penetrated the rust layer, then the electrochemical reactions take place on the surface of the pores (see Section 2.4). The specific area of the rust layer is then another critical parameter. The measured specific area of rust layers is very large, i.e. about 10 m^2/g (BET measurements on a 420-year-old rust powder), providing a potentially very large area for electrochemical reactions.

Thus, the commonly used porosity description (e.g. the cylindrical pores system) is unable to represent well the complex geometrical shape of the pores (Fig. 5) which is actually that of a large specific area associated with nanometric scale pores and low porosity volume (10%).

Just to complete the picture, since it will not be exploited further in the modelling, it can be mentioned that often two or three layers may be distinguished in a rust scales, differing in their relative amounts of oxides and oxy-hydroxides and porosity.

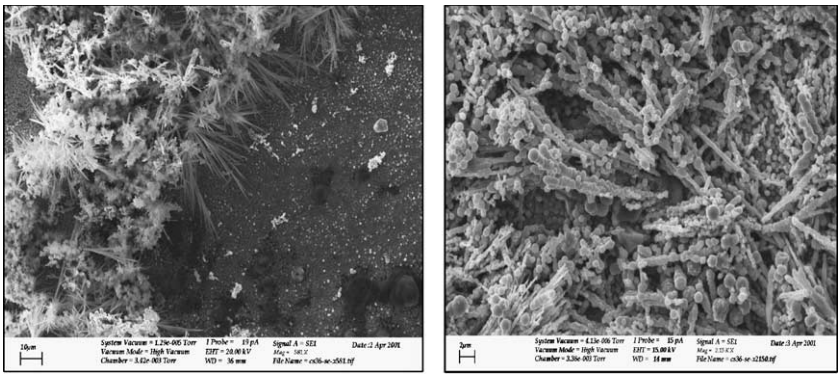

Fig. 5. SEM surface micrographs illustrating the complex geometry of the rusts layers (for more details see [26,27]).

Roughly, the first layer being more rich in α-FeOOH and compact (thus protective) and the second layer more γ-FeOOH rich and porous (thus non-protective). Sometimes, a third layer, mainly composed of incorporated dusts and very porous (with pores width many magnitude orders greater than those of the rust strictly speaking) is also observed.

To sum up, the simplified rust layer model is characterised by (Fig. 6)

- homogeneous composition in γ-FeOOH and α-FeOOH, the fraction of γ-FeOOH is given by β (∼0.2);
- thickness L (∼200 μm);
- porosity ε (∼10%), tortuosity τ (∼3) and specific area S_a (∼10 m^2/g).

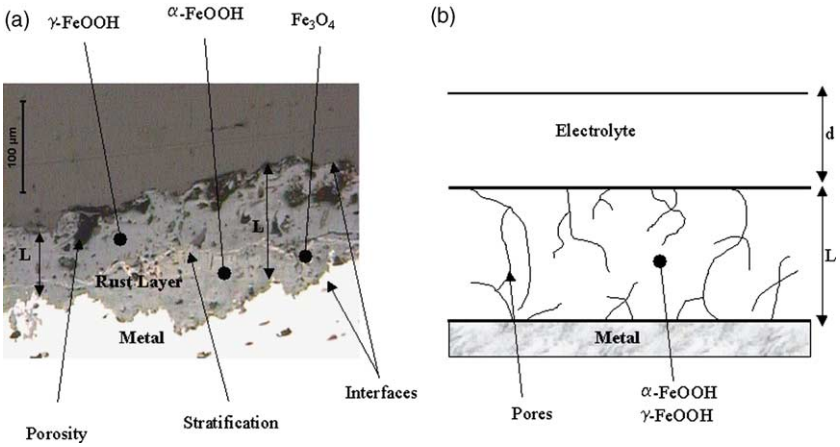

Fig. 6. The rust layer. (a) SEM micrograph of a 150-year-old rust layer (CC01 sample, see [26,27] for more details). (b) Sketch of the rust layer and the electrolyte film simplified models. L and d are the rust layer and electrolyte thickness, respectively.

The parameters L, β, ε and S_a can be measured [24,26–28,34], whereas τ is evaluated ($\tau \sim 3$) [36]. All the properties are assumed independent of space variables. As it can be seen, the chosen rust layer is an old one, with some hundred years of rusting. In the aim of long term prediction, the modelling considers not the development of AC on bare iron, but the progress of AC on a well grown rust layer.

The underlying metal is pure iron, no metal composition effects are then considered.

4. Modelling

The modelling of AC that is proposed is established on a modular basis.

A first module, focusing on thermo-hydraulic considerations is described in earlier publications [37,38]. The outputs of this modelling are the wet–dry cycle main features (electrolyte layer thickness, time of wetness, wetting and drying average duration) of a stored textbook well-defined metallic container according to climatic fluctuations. Basing on bilogarithmic laws [26,27] and an ISO standard approach this module can then provide some first results on predicting AC damage.

The second module, presented in this paper, is a mechanistic one, which is devoted to describing the physico-chemical phenomena occurring within the rust layer during a cycle. To begin with, only corrosion of pure iron is investigated (without taking into account specificities due, for instance, to alloying elements) and a typical wet–dry cycle is considered.

The link between the thermo-hydraulic and physico-chemical modules will be done later. The final aim of this modelling is to loop the physico-chemical module, provided cycle characteristics given by the thermo-hydraulic module, for a number of cycles (corresponding to a certain rusting time) in order to predict the long term damage of the container walls and the rust layer evolution.

4.1. Wetting stage

The first stage of the wet–dry cycle is described by considering that the amount of oxidised metal, and thus the damage, depends directly on the amount of γ-FeOOH reduced.

The rust layer being insulating at the beginning of the wet–dry cycle, the γ-FeOOH reduction begins at the metal surface and propagates through the rust layer, along the pore walls. It is considered that the reduction front moves forward by γ-FeOOH monolayer steps (on plans parallel to the metal). The process stops when the reduction front reaches the rust/electrolyte interface (Fig. 7).

It is supposed that all the γ-FeOOH present in the rust layer is reduced. It implies that all the γ-FeOOH islands are assumed to be in contact with the metal and that all the γ-FeOOH coats the pore walls with a some monolayers thick film. All the pores are also assumed to connect the metal with the electrolyte. Furthermore, it is assumed that all Fe[III] are reduced to Fe[II], without any modification of the crystallographic structure: There is a continuous path from γ-FeOOH to γ-Fe$\cdot$OH$\cdot$OH,

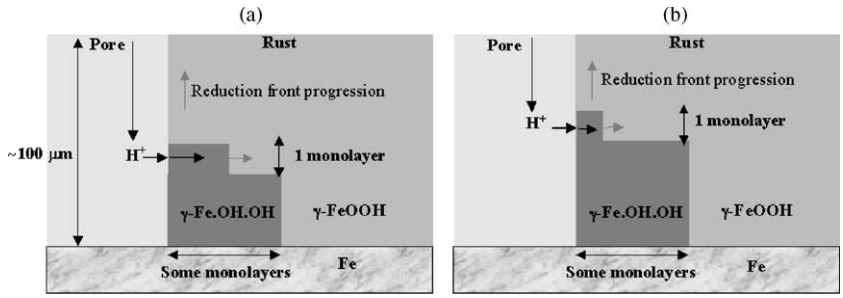

Fig. 7. Sketch of the progression of the reduction front. (a) A monolayer is "filled" from the pore wall to some monolayers deep. (b) When a plan of a monolayer thick and some monolayers deep is reduced, the plan above reduces in its turn, following the same process and thus progresses the reduction front.

without magnetite formation. However, experimental results show that, actually, all γ-FeOOH is not reduced after a wetting stage similar to those of natural wet–dry cycles. The modelling provides then an over-estimation of the damage.

It is assumed that the cathodic process determines the corrosion rate. The anodic process (metal dissolution and removal of the corrosion products by diffusion) is supposed sufficiently fast for the cathodic reaction to impose its rate.

As developed in Section 2.3, a Butler–Volmer law is used to describe γ-FeOOH reduction kinetics. H^+ diffusion inside γ-FeOOH is not considered as it occurs on only some monolayers and then is likely fast enough to maintain the H^+ concentration on reduction sites.

It is assumed that the reaction

$$\gamma\text{-FeOOH} + H^+ + e^- \xrightarrow{k} \gamma\text{-Fe}\cdot\text{OH}\cdot\text{OH} \tag{II}$$

leads to the formation of a solid solution γ-FeOOH/γ-Fe·OH·OH. The reduction current is thus given by

$$i_\gamma = F \cdot k[H^+]s_{\text{FeOOH}} \tag{2}$$

when assuming that i_γ is proportional to $[H^+]$ the H^+ concentration in the electrolyte (as H^+ diffusion inside the rust layer is not considered) and to s_{FeOOH}, the concentration of the surface sites (Fe[III] sites) where the reduction reaction takes place in a γ-FeOOH plan (Fig. 7). The rate constant of reaction (II) is k and F is the Faraday constant.

Diffusion of H^+ ions in the electrolyte, from the bulk reservoir to the surface of the pores, is supposed sufficiently fast for the $[H^+]$ to remain constant and homogenous. $[H^+]$ depends then only on the electrolyte pH. An apparent rate constant K, is then defined as

$$K = k[H^+]. \tag{3}$$

Let express s_{FeOOH} to obtain the γ-FeOOH reduction current.

The FeOOH surface sites density (on a plan cutting bulk FeOOH), N can be evaluated as follows:

$$N = \left(\frac{\rho}{M_{\mathrm{FeOOH}}} N_{\mathrm{Av}}\right)^{2/3} \tag{4}$$

with M_{FeOOH} the molar weight of γ-FeOOH and α-FeOOH, ρ the mean α- and γ-FeOOH densities and N_{Av} the Avogadro constant.

If a homogeneous mix of γ-FeOOH and α-FeOOH is assumed, the density of reducible sites (γ-FeOOH) is given by βN, with β the γ-FeOOH fraction of the rust layer.

The amount of reducible γ-FeOOH depends on the surface area of the pores, the composition of the rust layer (fraction of γ-FeOOH) and the thickness of γ-FeOOH that can be reduced.

The area of the pores is given by

$$S = S_{\mathrm{a}}(1-\varepsilon)\rho L, \tag{5}$$

where S_{a} is the measured specific area, ε the porosity, ρ the mean density of oxi-hydroxides and L the thickness of the rust layer.

Let consider the progression of the reduction front from the metal towards the rust/electrolyte interface. On a plan parallel to the metal, inside the rust layer, the area of reduced γ-FeOOH per surface unit is $L_{\mathrm{a}} \cdot n \cdot e$, with L_{a} the length of the pores per surface unit, n the number of γ-FeOOH monolayers that are reduced and e the thickness of one monolayer (Fig. 8).

The parameter L_{a} can be expanded as

$$L_{\mathrm{a}} = \frac{S}{L}. \tag{6}$$

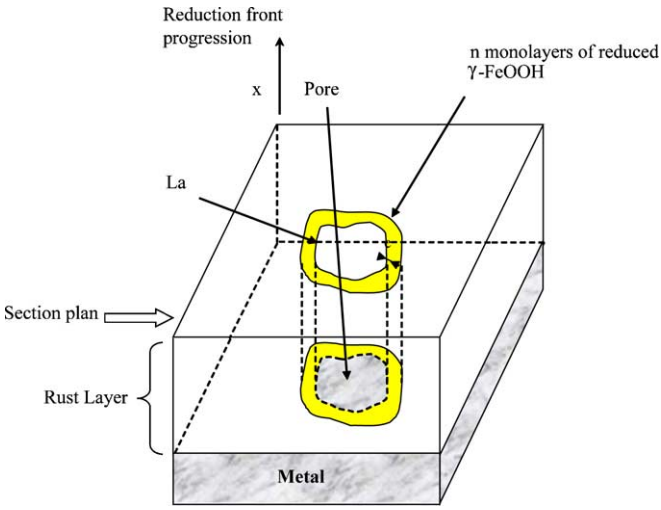

Fig. 8. Sketch of the progression of the reduction front of γ-FeOOH.

Incorporating the expressions of the different parameters, the γ-FeOOH reduction current density (with respect to the substrate area) Eq. (2) becomes then

$$i_\gamma = FK\frac{\beta \cdot N \cdot L_a \cdot n \cdot e}{N_{av}} = FK\frac{\beta \cdot N \cdot S \cdot n \cdot e}{L \cdot N_{av}}. \tag{7}$$

From this expression, it is possible to obtain a relationship that gives the propagation rate of the reduction front. When assuming that the reduction of γ-FeOOH progresses by plans parallel to the metal surface, dx, the distance by which the reduction front has progressed after the reduction of dn_γ moles of γ-FeOOH corresponds to $\frac{dx}{e}$ monolayers of γ-FeOOH. The amount dn_γ can be expressed as

$$dn_\gamma = \frac{L_a \cdot n \cdot e \cdot \beta \cdot N}{N_{av}}\frac{dx}{e}. \tag{8}$$

When replacing dn_γ in $i_\gamma = F\frac{dn_\gamma}{dt}$ by the previous expression and using (6), one obtains the progression rate of the reduction front v_R:

$$v_R = \frac{dx}{dt} = e \cdot K. \tag{9}$$

When all the parameters are independent of the space variables, then the time necessary to reduce a rust layer of thickness L is

$$\Delta t_R = \frac{L}{e \cdot K}. \tag{10}$$

About 2 h are necessary to reduce a rust layer of more than 100 μm thickness (say 200 μm) [32]. With a monolayer thickness of about 1 nm [39], it would give $K = 30$ s^{-1}.

The total amount of reduced γ-FeOOH is then $\frac{i_\gamma.\Delta t_R}{F} = \beta\frac{N.S.n}{N_{av}}$.

Assuming all the available γ-FeOOH is reduced when consuming the electrons produced by the oxidation of iron: $Fe \rightarrow Fe^{2+} + 2e^-$, the damage (or corrosion depth) is given by

$$p_\gamma = \beta\frac{N \cdot S \cdot n}{2N_{Av}}V_{Fe} \tag{11}$$

(with V_{Fe} the molar volume of iron) and the mean current density for a wetting stage that lasts Δt_R is then

$$i_\gamma = \beta\frac{F \cdot N \cdot S \cdot n}{\Delta t_R N_{Av}}. \tag{12}$$

Relations (11) and (12) are clearly overestimations as they consider the worst case: A rust layer composed of only γ-FeOOH and α-FeOOH species and where all the γ-FeOOH is reduced. Actually, it is likely that γ-FeOOH is not homogeneously dispersed in the rust layer (the outer density is different from the inner one, see Section 3.3) and all the surface γ-FeOOH is not in electrical contact with the metal and thus will not be reduced (there are more likely γ-FeOOH islands than a continuous

coating). The reduction current depends then on the spatial properties of the rust layer and would vary when the reduction front progresses through the rust layer.

4.2. Wet stage

When a sufficient amount of surface γ-FeOOH is reduced (wetting stage), the oxygen reduction becomes the prevailing cathodic reaction [16]. Indeed, oxygen can now be reduced on the conducting γ-Fe·OH·OH that coats the surface of the pores. Atmospheric oxygen is dissolved at the atmosphere/electrolyte interface. It is then, supposed that the dissolved oxygen diffuses first through the electrolyte and then through the pores of the rust (Fig. 9).

Oxygen is then reduced on the γ-Fe·OH·OH surface following the cathodic reaction:

$$O_2 + 4e^- + 2H_2O \xrightarrow{k} 4OH^- \quad \text{(VI)}$$

Reaction (VI) leads to an oxygen consumption which depletes oxygen concentration in the pores of the rust layer. It is supposed that this overall reaction is the elementary one that gives the rate of oxygen reduction.

The modelling is established as follows.

Only diffusion of dissolved oxygen, first through the electrolyte and then the pores, where there is an oxygen sink (the consumption of O_2 by reaction (VI)) is considered. With D_O the oxygen bulk diffusion coefficient, the 1-D mass balance equation for diffusive oxygen mass transport is, in the electrolyte:

$$\frac{\partial C}{\partial t} = D_O \frac{\partial^2 C}{\partial x^2}. \quad (13)$$

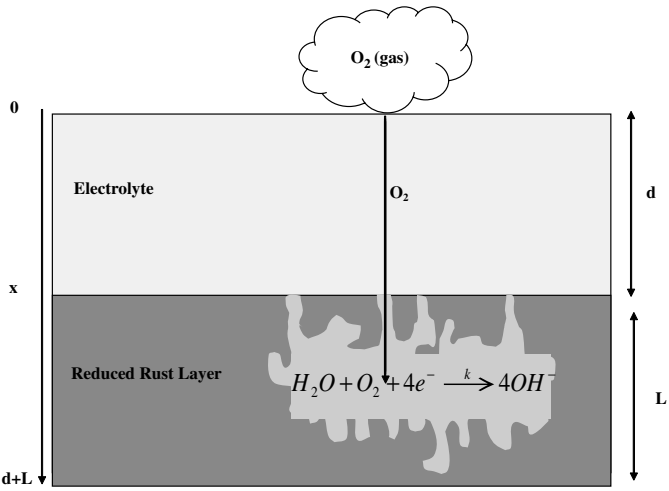

Fig. 9. Schematic representation of the oxygen reduction modelling. The electrolyte and rust layer thicknesses are d and L, respectively.

For diffusion inside the rust layer, the equivalent diffusion coefficient formalism is applied [36]. When assuming that porosity ε and tortuosity τ are independent of space variables, the equivalent oxygen diffusion coefficient D_{O}^{*}, is

$$D_{\mathrm{O}}^{*} = \frac{\varepsilon D_{\mathrm{O}}}{\tau}. \tag{14}$$

And the 1-D mass balance equation for diffusive oxygen mass transport in the rust layer is

$$\varepsilon \frac{\partial C}{\partial t} = D_{\mathrm{O}}^{*} \frac{\partial^2 C}{\partial x^2} - \beta \cdot s_{\mathrm{a}} V_{\mathrm{O}}. \tag{15}$$

The parameter V_{O} is the rate of oxygen reduction on γ-Fe$\cdot$OH$\cdot$OH surface:

$$V_{\mathrm{O}}(x) = k \cdot C(x) \tag{16}$$

with the approximation of a first order reaction. k is the rate constant of reaction (VI) and depends on the applied potential (E), the normal potential of O_2/OH^- couple ($E_{\mathrm{O}_2}^{0}$) and the standard rate constant of electrons exchange for this redox couple ($k_{\mathrm{O}_2}^{0}$).

$$k = k_{\mathrm{O}_2}^{0} \exp\left(-\frac{E - E_{\mathrm{O}_2}^{0}}{b_{\mathrm{C}}}\right). \tag{17}$$

As for the parameter s_{a}, it is area of the pores per volume unit:

$$s_{\mathrm{a}} = S_{\mathrm{a}}(1-\varepsilon)\rho \tag{18}$$

with S_{a} the specific area and ε the porosity of the rust layer and ρ the mean oxihydroxides density.

Assuming that all the γ-FeOOH was reduced during the wetting stage, then the area on which oxygen is reduced is $\beta \cdot s_{\mathrm{a}}$ per volume unit.

When the stationary state is reached, (13) and (15) are solved for the oxygen concentration in the pores $C(x)$:

$$C(x) = \frac{C_0}{1 + d/\lambda} \exp\left(-\frac{1}{\lambda}(x-d)\right) \quad x \in [d, L+d] \tag{19}$$

with the boundary condition: C_0 is the concentration of dissolved oxygen at the atmosphere/electrolyte interface (C_0 is given by Henry law), and continuity conditions at the electrolyte/rust layer interface. As with the parameter λ, it characterises the depth of oxygen penetration inside the rust layer and is defined by

$$\lambda = \sqrt{\frac{\varepsilon D_{\mathrm{O}}}{\tau \beta s_{\mathrm{a}} k}}. \tag{20}$$

Then, integrating (16) with (19) through all the rust layer and using the Faraday law, the oxygen reduction current i_{C} is given by the relation

$$i_{\mathrm{C}} = \beta \frac{\varepsilon}{\tau} \frac{4FD_{\mathrm{O}}C_0}{(d+\lambda)} \left(1 - \exp\left(-\frac{L}{\lambda}\right)\right). \tag{21}$$

Eq. (21) evaluates the oxygen reduction current density as a function of parameters describing the morphology of the rust layer (ε, τ, L) and parameters that are more related to the electrolyte properties (D, C_0, d). The current density is referred to the metallic substrate area and not to the real cathodic area of the rust layer.

To be more accurate, as long as the electrolyte thickness is larger than the diffusion layer width δ_O (Nernst diffusion layer), it is not d, the value of the electrolyte thickness that should be used in (21) and (23) but δ_O. During a large part of the wet stage, the electrolyte thickness is larger than δ_O. During this stage the potential is also close to constant [24]. The current is thus also constant and the corresponding damage p_O is

$$p_O = \frac{i_C}{2F} V_{Fe}. \tag{22}$$

As expected, λ is governed by competition between transport (ε, τ, D) and oxygen consumption processes (β, s_a, k). With experimental and literature values of these parameters, λ is evaluated as about 0.1 μm. The value of λ is then very small compared to the rust layer thickness ($L \sim 100$ μm) [26,27]. The dissolved oxygen almost does not penetrate inside the rust layer and is reduced at the extreme surface. Furthermore, λ is also small compared to the electrolyte thickness. Indeed, for the validity of the modelling, the electrolyte thickness should be greater than about 10 m; first to prevent precipitation processes and passivation and secondary because under a very thin electrolyte layer it appears that the rate determining step of oxygen reduction is no longer diffusion but solvation (see Section 2). Thus, in the validity range of the modelling, λ remains very small compared to the electrolyte layer and rust scale thicknesses (respectively d and L) and (21) can be simplified to

$$i_C = \beta \frac{\varepsilon}{\tau} \frac{4FD_O C_0}{d} \tag{23}$$

which is, except for the morphological factor $\frac{\varepsilon}{\tau}$, the expression of the limiting current that would have been obtained when considering diffusion limited oxygen reduction on a plane with a surface fraction β that is available for oxygen reduction. It agrees well with some experimental results showing a linear variation of oxygen reduction current with $\frac{1}{d}$ [6,10,15,17,18].

The corresponding damage would then be

$$p_O = \beta \frac{\varepsilon}{\tau} \frac{2D_O C_0}{\delta_O} V_{Fe} \Delta t_W \tag{24}$$

with Δt_W the time of the wet stage during which the electrolyte thickness is greater than δ_O.

The current remains then constant during the wet stage and at the beginning of the drying. The width δ_O is replaced by d when the electrolyte thickness becomes smaller than δ_O and leads to an increase of the reduction current. Eqs. (21) and (23) are then applicable for the beginning of the drying, until d reaches values of about

10 μm, when the passivation/precipitation begins and the cycle enters its last stage, the drying.

4.3. Drying

At the beginning of the drying, the decrease of the electrolyte thickness (thinner than 10 μm) leads to such an increase of the oxygen diffusion limiting current that it is no longer the rate of the cathodic reaction, but the rate of the anodic reaction that determines the corrosion rate. We will express the anodic current of iron oxidation.

It is considered that the reaction is under mixed transfer–diffusion control and that the rate of the reaction could be limited by the removal of the corrosion product.

The passivation-like phenomena (see Section 2.5) are represented by considering that the corrosion products are deposited on the anodic sites, which leads to the blocking of the dissolution sites and thus to the decrease of the oxidation current. The anodic sites blocking process is rendered by the following reactions:

$$Fe \rightarrow Fe^{2+} + 2e^{-} \tag{VII}$$

$$Fe^{2+} + 2OH^{-} = Fe(OH)_{2,S} \tag{VIII}$$

where reaction (VII) is the iron dissolution. Reaction (VIII) reproduces the blocking of the anodic sites with a deposit of iron hydroxide. It is neither real precipitation nor adsorption, but a modelling way to consider the blocking of the anodic sites when diffusion can no longer remove quickly enough the corrosion products due to a very rapid oxidation reaction (because potential becomes very anodic).

The decrease of the electrolyte volume during the drying leads to an increase of the corrosion products concentration and then to the blocking of the anodic sites (reaction (VIII)). The drop of the anodic current leads the system to progressively turn from a cathodic control to an anodic one. It is assumed that the covering by blocking species is made by one monolayer and that there is a complete blocking of the sites when the coverage ratio is equal to 1.

It is supposed that the only charged species present in the pores are Fe^{2+} and OH^{-}. The solution pH is then fixed by the solubility of $Fe(OH)_2$. A possible increase of the pH inside the rust layer due to the cathodic reaction (reduction of O_2) that could help the passivation of iron in a more alkaline solution is then not considered.

As the "macroscopic" electrolyte model is used, the pore volume is neglected. The limits of the model (Fe^{2+} saturation) are then reached a bit faster than if the pore volume was considered.

The modelling considers only the stage of the drying that comes with electrochemical reactions, i.e. that there is sufficiently electrolyte at the surface. The re-oxidation of the rust layer at the end of the drying that allows the γ-FeOOH to regenerate for the next cycle is then not modelled.

The iron oxidation current is given by the flux of Fe^{2+} produced at the metal/electrolyte interface at the bottom of the pores. This flux is determined by the diffusion and migration of Fe^{2+} from the anodic sites to the bulk electrolyte, out of the

rust layer. The mass transport of Fe^{2+} through nanometric scale pores is likely very different of what it is in a bulk electrolyte. The mass transport of Fe^{2+} is rendered by a formalism identical to bulk diffusion, with the same diffusion coefficient. The corrections due to nanometric pores and electric field are introduced by an equivalent diffusion length δ_{Fe}, used like the thickness of a Nernst layer in bulk electrolyte.

The iron oxidation current density i_A is then

$$i_A = \varepsilon \frac{2FD_{Fe}}{\delta_{Fe}}(C_S - C) \tag{25}$$

with F the Faraday constant, D_{Fe} the Fe^{2+} bulk diffusion coefficient, C_S and C respectively the Fe^{2+} surface and bulk concentrations.

The current density is referred to the substrate area kept free by the rust layer by assuming that the fraction of the surface not covered by rust is equal to the porosity ε (it is rigorously right only in the case of non-tortuous cylindrical pores perpendicular to the surface).

The limiting diffusion current i_{LA} is reached when the surface concentration is equal to the saturation concentration:

$$i_{LA} = \varepsilon \frac{2FD_{Fe}}{\delta_{Fe}}(C_{sat} - C) = \varepsilon \frac{2FD_{Fe}}{\delta_{Fe}} C_{sat}(1 - s) \tag{26}$$

with C_{sat} the Fe^{2+} saturation concentration and s the deviation from saturation.

$$s = \frac{C}{C_{sat}}. \tag{27}$$

From these expressions, a relation between surface and bulk Fe^{2+} concentrations is obtained:

$$\frac{C_S}{C_{sat}} = s + \frac{i_A}{i_{LA}}(1 - s). \tag{28}$$

With reactions (VII) and (VIII), the anodic current density i_A can be written as

$$i_A = \varepsilon 2Fk^0_{Fe}(1 - \theta)\exp\left[\frac{E - E^0_{Fe}}{b_A}\right] = \varepsilon i_{0A}(1 - \theta)\exp\left[\frac{E - E^0_{Fe}}{b_A}\right] \tag{29}$$

with k^0_{Fe} the standard rate constant of electrons exchange, E^0_{Fe} the normal potential of the redox couple Fe^{2+}/Fe, b_A the Tafel coefficient for iron oxidation and θ the coverage ratio. i_{0A} is defined as $i_{0A} = 2Fk^0_{Fe}$.

When, for purposes of simplicity, it is assumed that the coverage ratio of the anodic sites is proportional to Fe^{2+} concentration at the metal/electrolyte interface and that the surface is completely covered by a monolayer of $Fe(OH)_2$ when the Fe^{2+} concentration is equal to the saturation concentration ($\theta = 1$ for $C_S = C_{sat}$), then

$$\theta = \frac{C_S}{C_{sat}}. \tag{30}$$

Using the relations between C_S and C_{sat} (28) and (30) in the expression of the anodic current (29), the iron oxidation current writes then

$$i_A = \frac{\varepsilon i_{0A}(1-s)\exp\left[\dfrac{E-E^0_{Fe}}{b_A}\right]}{1+\dfrac{\varepsilon i_{0A}}{i_{LA}}(1-s)\exp\left[\dfrac{E-E^0_{Fe}}{b_A}\right]}. \quad (31)$$

This provides the expression of anodic current as a function of the electrode potential and Fe^{2+} bulk concentration. This relation can be used only as long as the Fe^{2+} concentration is inferior the precipitation limit ($s < 1$).

The assumptions chosen lead to consider that the metal is completely covered with blocking species when the $Fe(OH)_2$ precipitation limit is reached and that there is then no more metal free (and no more corrosion). This corresponds then to the end of the drying stage, as defined in the model (indeed, there is still electrolyte in the pores, and although there is no more electrochemical reactions leading to the oxidation of iron, the corrosion products are still reacting, for instance through the reoxidation of γ-FeOOH [8]).

The thickness d of the electrolyte is decreasing because of the drying, the Fe^{2+} concentration is then increasing and can be written:

$$C = C_{Fe}\frac{d_0}{d}. \quad (32)$$

This relation leads to

$$s = \frac{C_{Fe}}{C_{sat}}\frac{d_0}{d} \quad (33)$$

which, by replacing in (31), provides the current variation as a function of the potential and the thickness of the electrolyte. This expression is usable as long as $s < 1$ ($C < C_{sat}$).

Above, $C = C_{sat}$ whatever d and E are, the anodic sites are covered by a blocking species film. There is no more anodic dissolution. It is the end of the wet–dry cycle, as described by the modelling (but not the end of the actual wet–dry cycle).

When the potential becomes more anodic, iron oxidation current is controlled by the corrosion products removal. When the electrolyte thickness decreases, the Fe^{2+} concentration is closer to saturation, the passivity current is smaller and the limiting current is reached quickly (Fig. 10).

5. Synthesis—discussion

5.1. Each stage

All the parameters values are listed in Table 2. For a summary of the equations, see Table 3 and for electrochemical reactions, see Table 4.

5.1.1. Lepidocrocite reduction

The maximum damage is $p_\gamma = 0.16$ μm and the mean current density is $i_\gamma = 65$ μA/cm^2. These results correspond to a corrosion rate of 10 μm/yr (when considering

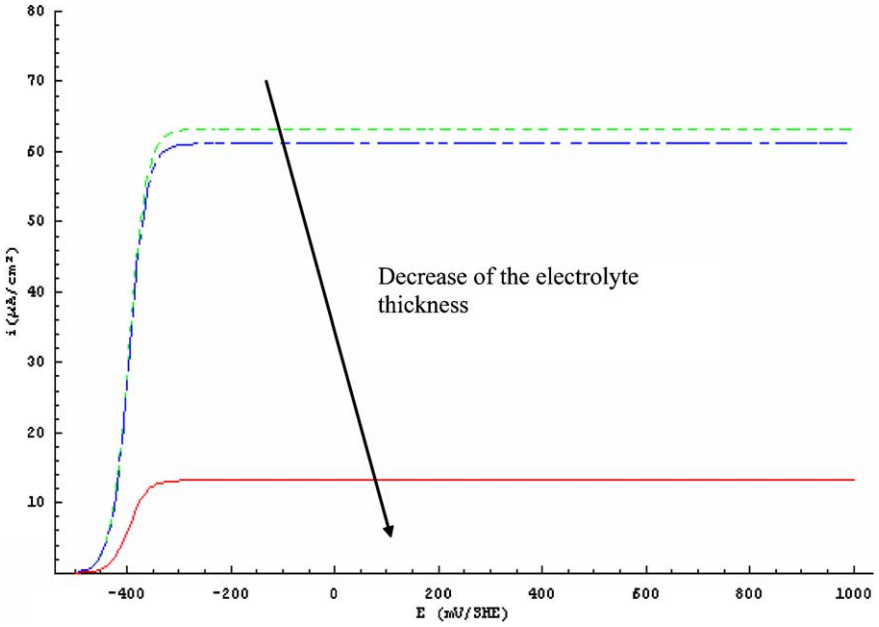

Fig. 10. Current–potential curve, for different values of the electrolyte thickness: 200 μm (dotted line), 100 μm (dot-dashed line), 10 μm (solid line).

100 c/yr), due only to the γ-FeOOH reduction. Experimental results [2] give the same damage order of magnitude, but for complete wet–dry cycles, whereas only γ-FeOOH reduction is considered here.

Nevertheless, on fresh rust layers, thus with high porosity and composed of nearly only γ-FeOOH, when taking values closer to that situation (i.e. $\varepsilon = 0.3$, $S_a = 30\ m^2/g$ and $\beta = 0.9$), the model results are of the same order of magnitude as the experimental ones (with the preceding values, $i_\gamma = 680\ \mu A/cm^2$ and $p_\gamma = 1.7\ \mu m$) [8,32].

For old rust layers, the model overestimates the damage because it considers an ideal γ-FeOOH reduction (all the γ-FeOOH is reduced), which leads to a maximised damage. The model corresponds then more the case of fresh rust. This is to be related to experimental results that exhibit a dramatic slow-down of the corrosion rate with time (thus passing from fresh to old rust layers) [40,41].

The rate of lepidocrocite reduction is supposed directly proportional to the electrolyte pH. Because of the "macroscopic" electrolyte model and to ease the mathematical treatment, the pH is supposed constant in time. This assumption is partly based on the experimental observations of Nishikata et al. [17]. Indeed, he observed an effect of pH on the atmospheric corrosion rate of iron only under a very thick electrolyte layer (>1 mm) and for a short exposure period (<1 h). For longer exposure the effect of pH was negligible, probably due to neutralization of electrolyte layer by the progress of corrosion reactions. Our modelling is basically in this condition: thick electrolyte and relatively long exposure time.

Table 2
Table of symbols

Latin letters			
b_A	Tafel coefficient for iron oxidation.	measured	40 mV
b_C	Tafel coefficient for oxygen reduction	measured [19]	48 mV
C	bulk O_2 or Fe^{2+} concentrations	calculated	mol/m^3
C_{Fe}	bulk concentration Fe^{2+} at the beginning of the drying,	evaluated	10^{-4} mol/m^3
C_S	Fe^{2+} surface concentration	calculated	mol/m^3
C_{sat}	Fe^{2+} saturation concentration	calculated [3]	4.2×10^{-3} mol/m^3
C_0	O_2 concentration at atmosphere/ electrolyte interface	table	0.25 mol/m^3
D_{Fe}	Fe^{2+} bulk diffusion coefficient	table	0.72×10^{-9} m^2/s
D_O	O_2 diffusion coefficient in the electrolyte	table	1.9×10^{-9} m^2/s
D_O^*	equivalent oxygen diffusion coefficient	calculated (14)	m^2/s
d	electrolyte thickness	measured	~100 μm and >10 μm
d_0	electrolyte thickness at the beginning of the drying.		μm
E	electrode potential		V/SHE
E^0_{Fe}	normal potential of the Fe^{2+}/Fe redox couple	table	−440 mV/SHE
$E^0_{O_2}$	normal potential of the O_2/OH^- redox couple	table	750 mV/SHE
e	thickness of one γ-FeOOH mono-layer	table [39]	~1 nm
F	Faraday constant	constant	96,500 C/mol
i_A	iron oxidation current density	calculated (31)	A/m^2
i_C	O_2 reduction current density	calculated (21) and (23)	1.2 μA/cm^2
i_{LA}	limiting diffusion current	calculated (26)	A/m^2
i_{0A}	''iron corrosion current''	calculated	0.5 A/m^2
i_γ	γ-FeOOH reduction current	calculated (7) and (12)	65 μA/cm^2
K	apparent rate constant of reduction γ-FeOOH	evaluated (10)	30 s^{-1}
k	rate constant of electrochemical reactions		
$k^0_{O_2}$	standard rate constant of electrons exchange for O_2	measured [20]	10^{-10} m/s
k^0_{Fe}	standard rate constant of electron exchange for Fe^{2+}/Fe	measured	10^{-7} mol/s/m^2
L	rust layer thickness	measured	~200 μm
L_a	length of the pores per surface unit	calculated (6)	m^{-1}
N	density of FeOOH surface site	calculated (4)	1.86×10^{18} site/m^2
N_{Av}	Avogadro constant	constant	6.023×10^{23}
N_c	number of wet–dry cycles		
M_{FeOOH}	molar weight of FeOOH	constant	89 g/mol
n	number of reduced monolayer of γ-FeOOH	evaluated [20]	2
n_γ	number of γ-FeOOH moles		moles
p	total damage of a wet–dry cycle	calculated	μm
p_O	damage due to O_2 reduction	calculated (22) and (24)	0.008 μm
p_γ	damage due to γ-FeOOH reduction	calculated (11)	0.16 μm

Table 2 (*continued*)

Latin letters			
S	area of the pores per surface unit	calculated (5)	15,120
S_a	specific area of the rust	measured	10 m^2/g
s	deviation from Fe^{2+} saturation	calculated (27) and (33)	
s_a	surface of the pores per volume unit	calculated (18)	7.38×10^{7} m^{-1}
s_{FeOOH}	γ-FeOOH surface sites concentration	calculated	site/m^2
V_{Fe}	molar volume of iron	constant	7.1×10^{-6} m^3/mol
v_R	rate of the γ-FeOOH reduction front progression	calculated (9)	m/s
V_O	rate of oxygen reduction	calculated (16)	mol/m^2/s
Greek letters			
β	fraction of γ-FeOOH	measured (1)	0.2
Δt_R	duration of the wetting stage	evaluated (10)	2 h
Δt_W	duration of the wet stage	evaluated	5 h
δ_{Fe}	equivalent diffusion length for Fe^{2+}	evaluated	0.1 μm
δ_O	diffusion length for O_2	evaluated	~100 μm
ε	porosity of the layer	measured	10%
θ	coverage ratio in blocking species on the metal	calculated (30)	
λ	depth of O_2 penetration	calculated (20)	0.1 μm
ρ	mean α- and γ-FeOOH density	table/evaluated	4.2×10^{6} g/m^3
τ	tortuosity of the rust layer	evaluated	3

For calculated values, number in brackets gives the formula used.

This pH shift is also responsible for the formation of magnetite. However, in a first approach, a two-constituent rust layer (i.e. simplified in terms of modelling) has been considered, using lepidocrocite and goethite as representative of the receptively active and protective properties of the different constituents of a real rust layer. The formation of magnetite with the pH increase has not been considered because it has no consequence on the corrosion rate during the first stage (lepidicrocite reduction).

5.1.2. Oxygen reduction

When considering only the wet stage (i.e. when electrolyte thickness and potential are constant), a value of oxygen reduction current of $i_C = 1.2$ μA/cm^2 is obtained. It is of the same order of magnitude as the published values [17,32,35]. The corresponding damage for a wet stage of 5 h is $p_O = 0.008$ μm, which corresponds to about 1 μm/yr and is also quite reasonable.

For the modelling, it was considered that λ (~0.1 μm) is negligible face to both rust layer ($L \sim 100$ μm) and the electrolyte ($d > 10$ μm) thicknesses. This is indeed verified for the typical conditions of AC as shown in Fig. 11.

The main conclusion of this first approach of oxygen reduction modelling is that there is nearly no penetration of the dissolved oxygen inside a thick and fully reduced rust layer, as supposed for the formalisation of the modelling. In this case, oxygen is quickly reduced on the outer part of the rust layer, at the entrance of the pores. This leads to an oxygen reduction rate nearly independent from the rust thickness. When the rust layer is partially reduced (only the inner part), it increases the diffusion path

Table 3
Table of equations

(1)	$\beta = \frac{\gamma}{\alpha+\gamma} = \frac{1}{1+\frac{\alpha}{\gamma}}$	(2)	$i_\gamma = F \cdot k[\mathrm{H}^+] s_{\mathrm{FeOOH}}$
(3)	$K = k[\mathrm{H}^+]$	(4)	$N = \left(\frac{\rho}{M_{\mathrm{FeOOH}}} N_{\mathrm{Av}}\right)^{2/3}$
(5)	$S = S_{\mathrm{a}}(1-\varepsilon)\rho L$	(6)	$L_{\mathrm{a}} = \frac{S}{L}$
(7)	$i_\gamma = FK\frac{\beta \cdot N \cdot L_{\mathrm{a}} \cdot n \cdot e}{N_{\mathrm{av}}} = FK\frac{\beta \cdot N \cdot S \cdot n \cdot e}{L \cdot N_{\mathrm{av}}}$	(8)	$\mathrm{d}n_\gamma = \frac{L_{\mathrm{a}} \cdot n \cdot e \cdot \beta \cdot N}{N_{\mathrm{av}}}\frac{\mathrm{d}x}{e}$
(9)	$v_R = \frac{\mathrm{d}x}{\mathrm{d}t} = e \cdot K$	(10)	$\Delta t_R = \frac{L}{e \cdot K}$
(11)	$p_\gamma = \beta\frac{N \cdot S \cdot n}{2N_{\mathrm{Av}}} V_{\mathrm{Fe}}$	(12)	$i_\gamma = \beta\frac{F \cdot N \cdot S \cdot n}{\Delta t_R N_{\mathrm{Av}}}$
(13)	$\frac{\partial C}{\partial t} = D_{\mathrm{O}}\frac{\partial^2 C}{\partial x^2}$	(14)	$D^*_{\mathrm{O}} = \frac{\varepsilon D_{\mathrm{O}}}{\tau}$
(15)	$\varepsilon\frac{\partial C}{\partial t} = D^*_{\mathrm{O}}\frac{\partial^2 C}{\partial x^2} - \beta \cdot s_{\mathrm{a}} V_{\mathrm{O}}$	(16)	$V_{\mathrm{O}}(x) = k \cdot C(x)$
(17)	$k = k^0_{\mathrm{O}_2}\exp\left(-\frac{E - E^0_{\mathrm{O}_2}}{b_{\mathrm{C}}}\right)$	(18)	$s_{\mathrm{a}} = S_{\mathrm{a}}(1-\varepsilon)\rho$
(19)	$C(x) = \frac{C_0}{1+d/\lambda}\exp\left(-\frac{1}{\lambda}(x-d)\right)$	(20)	$\lambda = \sqrt{\frac{\varepsilon D_{\mathrm{O}}}{\tau\beta s_{\mathrm{a}} k}}$
(21)	$i_{\mathrm{C}} = \beta\frac{\varepsilon}{\tau}\frac{4FD_{\mathrm{O}}C_0}{(d+\lambda)}\left(1-\exp\left(-\frac{L}{\lambda}\right)\right)$	(22)	$p_{\mathrm{O}} = \beta\frac{i_{\mathrm{C}}}{2F} V_{\mathrm{Fe}}$
(23)	$i_{\mathrm{C}} = \beta\frac{\varepsilon}{\tau}\frac{4FD_{\mathrm{O}}C_0}{d}$	(24)	$p_{\mathrm{O}} = \beta\frac{\varepsilon}{\tau}\frac{2D_{\mathrm{O}}C_0}{d} V_{\mathrm{Fe}}\Delta t_{\mathrm{W}}$
(25)	$i_{\mathrm{A}} = \varepsilon\frac{2FD_{\mathrm{Fe}}}{\delta_{\mathrm{Fe}}}(C_{\mathrm{S}} - C)$	(26)	$i_{\mathrm{LA}} = \varepsilon\frac{2FD_{\mathrm{Fe}}}{\delta_{\mathrm{Fe}}}(C_{\mathrm{sat}} - C) = \varepsilon\frac{2FD_{\mathrm{Fe}}}{\delta_{\mathrm{Fe}}}C_{\mathrm{sat}}(1-s)$
(27)	$s = \frac{C}{C_{\mathrm{sat}}}$	(28)	$\frac{C_{\mathrm{S}}}{C_{\mathrm{sat}}} = s + \frac{i_{\mathrm{A}}}{i_{\mathrm{LA}}}(1-s)$
(29)	$i_{\mathrm{A}} = \varepsilon i_{0\mathrm{A}}(1-\theta)\exp\left[\frac{E - E^0_{\mathrm{Fe}}}{b_{\mathrm{A}}}\right]$	(30)	$\theta = \frac{C_{\mathrm{S}}}{C_{\mathrm{sat}}}$
(31)	$i_{\mathrm{A}} = \frac{\varepsilon i_{0\mathrm{A}}(1-s)\exp\left[\frac{E - E^0_{\mathrm{Fe}}}{b_{\mathrm{A}}}\right]}{1 + \frac{\varepsilon i_{0\mathrm{A}}}{i_{\mathrm{LA}}}(1-s)\exp\left[\frac{E - E^0_{\mathrm{Fe}}}{b_{\mathrm{A}}}\right]}$	(32)	$C = C_{\mathrm{Fe}}\frac{d_0}{d}$
(33)	$s = \frac{C_{\mathrm{Fe}}}{C_{\mathrm{sat}}}\frac{d_0}{d}$	(34)	$\beta = 0.6\exp\left(-\frac{N_{\mathrm{c}}}{100,000}\right)$

Table 4
Table of reactions

(I)	$4\mathrm{Fe} + 3\mathrm{O_2} + 2\mathrm{H_2O} = 4\mathrm{FeOOH}$
(II)	$\gamma\text{-FeOOH} + \mathrm{e^-} + \mathrm{H^+} \rightarrow \gamma\text{-Fe}\cdot\mathrm{OH}\cdot\mathrm{OH}$
(III)	$3\gamma\text{-FeOOH} + \mathrm{H^+} + \mathrm{e^-} \rightarrow \mathrm{Fe_3O_4} + 2\mathrm{H_2O}$
(IV)	$\mathrm{O_2} + 2\mathrm{H_2O} + 2\mathrm{e^-} = \mathrm{H_2O_{2,S}} + 2\mathrm{OH^-}$
(V)	$\mathrm{H_2O_{2,S}} \rightarrow \frac{1}{2}\mathrm{O_2} + \mathrm{H_2O}$
(VI)	$\mathrm{O_2} + 4\mathrm{e^-} + 2\mathrm{H_2O} \rightarrow 4\mathrm{OH^-}$
(VII)	$\mathrm{Fe} \rightarrow \mathrm{Fe^{2+}} + 2\mathrm{e^-}$
(VIII)	$\mathrm{Fe^{2+}} + 2\mathrm{OH^-} = \mathrm{Fe(OH)_{2,S}}$

of oxygen, causing a decrease in the oxygen reduction rate when increasing rust thickness. The diffusion of oxygen through the pores has then to be examined in more details. The morphological properties of the pores are very complex [16,26,27]

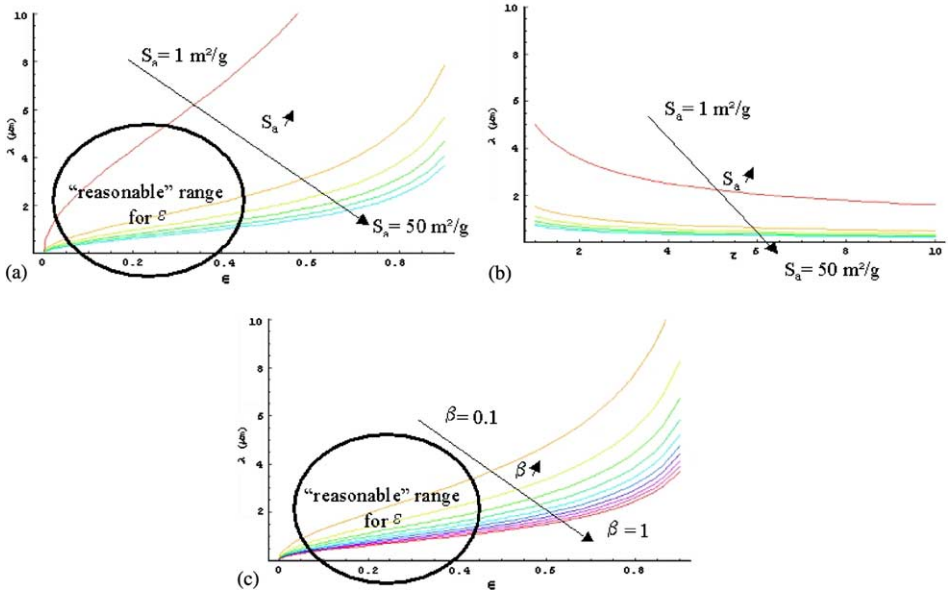

Fig. 11. Effect of different parameters on the depth of oxygen penetration (λ). (a) Variation of λ with porosity ε for different values of specific area S_a. (b) Variation of λ with tortuosity τ for different values of S_a. (c) Variation of λ with ε for different values of lepidocrocite fraction β (with $\varepsilon = 0.1$, $\tau = 3$, $S_a = 10$ m^2/g, $\beta = 0.2$ when they are considered as parameters).

and may play an important role in the diffusion of oxygen that needs to be included into a more realistic model of rust layer.

5.1.3. Blocking of the anodic sites

Before examining the restrictions of the model, comments on some parameter values are required.

Experimental investigations on ancient iron (samples from CV01 see [26,27]) have given electrochemical data for iron oxidation:

- $k^0_{Fe} \approx 10^{-7}$ mol/s/m^2 (a value of 10^{-6} mol/s/m^2 can be extracted from literature data [10,42]);
- $b_A \approx 40$ mV (to be compared with $\beta_A = 17.4$ mV given in [3, p. 528]).

The value of the saturation concentration in Fe^{2+} species is obtained when considering that there is only Fe^{2+} and OH^- species in solution. Electroneutrality and precipitation equilibrium of $Fe(OH)_2$ ($\log[Fe^{2+}] = 11.36 - 2pH$ [43]) give then a pH of 8.37 and $C_{sat} = 4.2 \times 10^{-3}$ mol/m^3.

δ_{Fe} is an equivalent diffusion path that allows to use classical diffusion formalism. From [42] and using Eqs. (26) and (33), it can be evaluated as $\delta_{Fe} \approx 0.1$ μm.

The Fe^{2+} concentration at the beginning of the drying, C_{Fe}, is more tricky. Indeed, when considering a damage of about 0.2 μm for the two first stages of the wet–dry

cycle (as given by the model), it corresponds to 0.03 mol/m^2 of Fe^{2+} released in solution. This would lead to a bulk concentration of about 100 mol/m^3 in a 300 μm thick electrolyte. This concentration is largely superior to Fe^{2+} precipitation limit (C_{sat}). It may then be assumed that the main part of Fe^{2+} released by iron oxidation during the first stages of the wet–dry cycle is already under hydroxide form at the beginning of the drying. With results from [42], a C_{Fe} value of 10^{-4} mol/m^3 can be evaluated. This value also leads to a maximum current value for an electrolyte thickness of about 10 μm (Fig. 13) which agrees with experimental results [10,15–18].

A maximum current density is expected when the depth of oxygen penetration λ is no longer negligible compared to the electrolyte thickness, i.e. for $d \sim 0.1$ μm. Then, an order of magnitude for the current density of about 1 mA/cm^2 could be expected, agreeing with those reported [7]. However, the model does not allow reaching such a stage, the complete blocking of the sites occurring before. This shows the limitations of this part of the model as discussed below.

As concerning the modelling assumptions, the blocking of anodic sites by a ferrous hydroxide deposit is only a simulation of the actual process, far more complex. It aims to bring in the modelling a passivation-like mechanism during the drying. This modelling has the advantage to give easily an analytic form. But it is also quite restrictive because it leads to consider that all the sites are blocked when a monolayer of corrosion product is deposited. It neither takes into consideration the possibility to form gel-like corrosion products in the pores that hinder mass transport, but does not block immediately and completely the anodic sites. The actual blocking of the sites would then take place later and less abruptly than in the modelling.

Moreover, the pore volume is not considered in the modelling. For a given electrolyte thickness (above the outer surface of the rust layer), the actual electrolyte volume (comprising the volume of the pores) is greater than in the modelling. The precipitation and blocking of the anodic sites, and then the end of the electrochemical corrosion, occur actually later than they do in the modelling.

The modelling considers also that there are in solution only Fe^{2+} and OH^- ions. But it is possible to oxidise Fe^{2+} into Fe^{3+}, far less soluble (especially at the end of the drying, when the potential becomes more oxidising). This modifies then the equilibriums between species that may block the anodic sites.

More, it must be reminded that the likely effect of a pH increase (due to oxygen reduction), the favouring of iron passivation, is not considered in the modelling. Indeed, this part of the modelling is not based on actual observations. The hydrolysis of the Fe^{2+} ions is just a simulation of a more complex and unknown process of blocking of the anodic sites. The subsequent variation in pH that could be expected from reactions (VII) and (VIII) is then not considered, as well as any other likely change in the electrolyte composition during this stage. The model only focuses on the progressive blocking of the anodic sites.

Finally, the blocking of the sites, as described in the modelling, depends on both potential and bulk Fe^{2+} concentration. The electrolyte volume plays then an important role and is used as parameter to control the modelling. To simplify, an homogeneous electrolyte film of variable thickness is considered. This description is acceptable for relatively thick electrolytes (100 μm) that can be found during the wet

stage. But, during the end of the drying, the electrolyte is likely splitting in droplets. This phenomenon is amplified by the porous structure of the rust layer and by the acicular morphology of some crystallites (Fig. 5), that yields a very complex repartition of the electrolyte at the end of the drying. These phenomena were not considered for the modelling because the damage during the last moments of the drying is negligible compared to whole wet–dry cycle. Nevertheless, in the case of thick and porous rust layer it is likely that a major part of the drying phenomena occurs inside the pores of the rust layer. The notion of a plane electrolyte should then be revised for further modelling.

5.2. Whole wet–dry cycle

In this section oxygen reduction and blocking sites models are synthesised to obtain a global modelling of the wet stage and the beginning of the drying.

Whereas during the wetting and the wet stage it is mainly the cathodic reactions (γ-FeOOH reduction and then O_2 reduction) that control the iron corrosion rate, during the drying, it is the anodic reaction that is limiting. In the modelling, it is the increase of Fe^{2+} concentration during the drying as well as the anodic shift of the potential that lead to the blocking of the anodic sites, to the diminishing of the anodic current and finally to the end of any electrochemical corrosion.

If it is assumed that during the drying (or at least during a long part of it), it is not the oxygen solvation that limits oxygen reduction, but that it is still under transfer–diffusion control (which is true as long as there is a sufficiently thick electrolyte film i.e. $d > 10$ μm), it is possible to fuse the models developed for oxygen reduction during the wet stage and iron oxidation during the drying. This modelling describes the variations of the corrosion current during the wet and drying stages until the complete blocking of the anodic sites.

The corrosion current is determined by the equality between reduction and oxidation currents, which in turn fixes the value of the electrode potential (Fig. 12). The equality of relations (21) and (31) gives then the corrosion current and the electrode potential. These equations, in the validity range of the modelling, can be used for the wet stage (current mainly determined by the cathodic branch) and the drying (current mainly determined by the anodic branch at the end of then drying).

This provides the current variations as a function of the electrolyte thickness (Fig. 13). When the electrolyte thickness decreases, the oxygen diffusion limiting current increases, the anodic current follows, it results then an increase of the corrosion current. It goes on, until the anodic current, which decreases with the electrolyte because of the blocking of the anodic sites, can no longer do with the cathodic current. The system then turns to anodic control and the corrosion current decreases until the final stop of the electrochemical corrosion. With the modelling hypotheses, the end of electrochemical corrosion comes when Fe^{2+} ions reach their precipitation limit and the anodic surface is fully blocked.

Fig. 14 gives the variation of the corrosion current as a function of the potential during the wet and the drying stages of a wet–dry cycle. The anodic shift of the electrode potential with the drying helps the re-oxidation of reduced species within

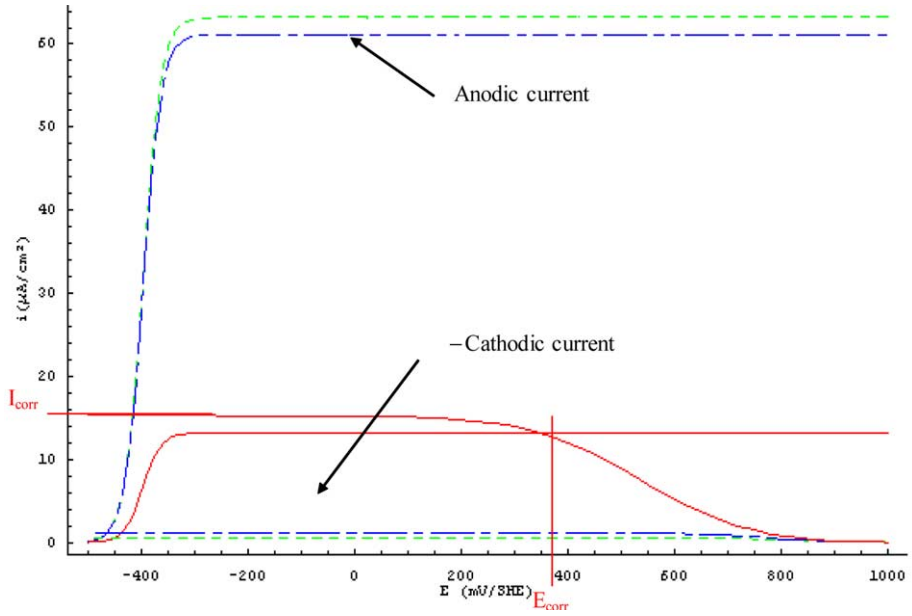

Fig. 12. Current–potential curves of the anodic current (i_A) and cathodic one ($-i_C$) for different values of the electrolyte thickness (200 μm: dotted line, 50 μm: dot-dashed line, 10 μm: solid line).

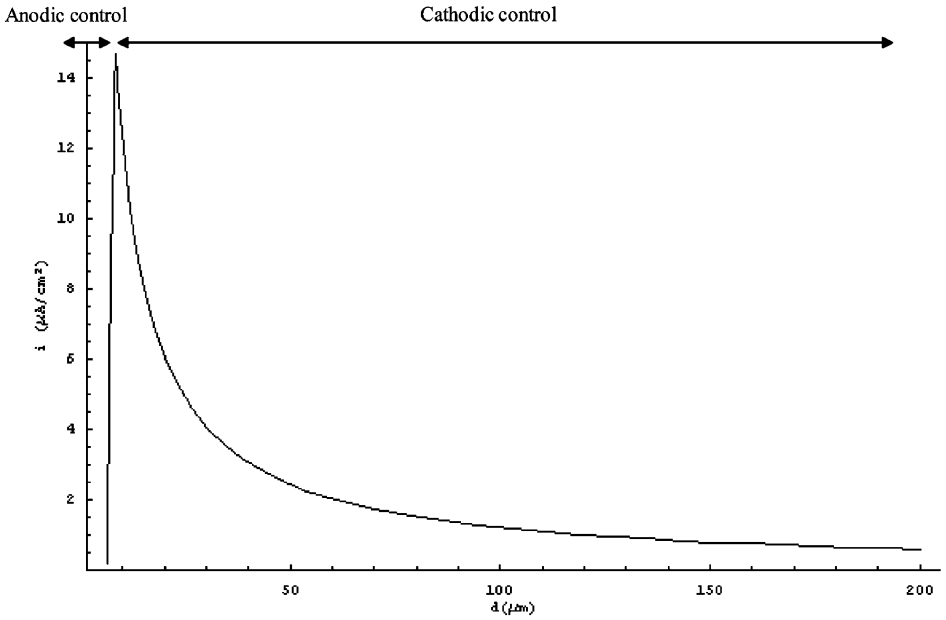

Fig. 13. Variation of the corrosion current as a function of the electrolyte thickness.

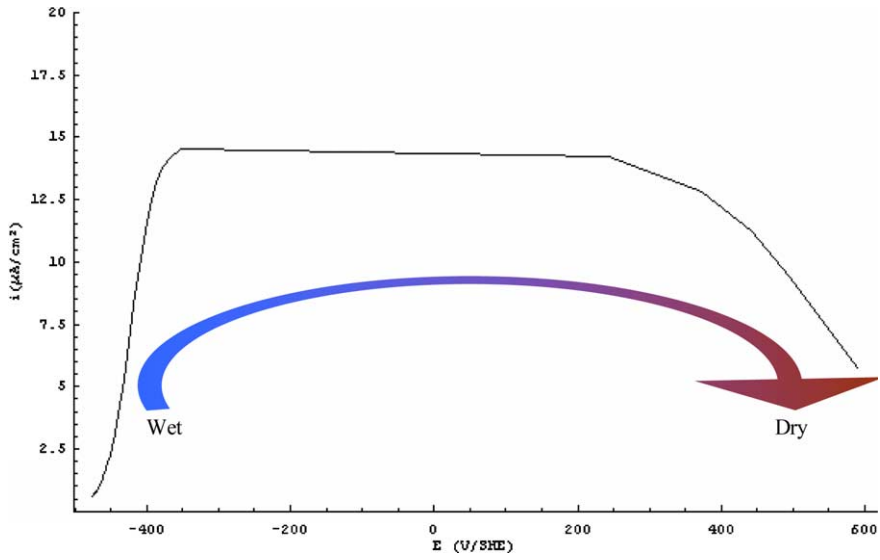

Fig. 14. Variation of the current as a function of the electrode potential during a wet–dry cycle.

the rust layer, notably γ-FeOOH, reduced during the wetting. It regenerates the active species, γ-FeOOH, for the next wet–dry cycle.

The reduction of the γ-FeOOH during the wetting stage is the first step of the modelling, it prepares the rust layer (formation of reduction sites for O_2 in the rust layer) for the following stages: The wet stage and the beginning of the drying are then modelled as presented above. The modelling of the end of the drying is not yet developed because it is mainly re-oxidation of the rust layer and causes then little damage to the metal.

5.3. Long term behaviour

As shown in the previous sub-sections, the modelling is able to predict reasonable behaviours (order of magnitude of the damage and current–potential evolution), for a typical wet–dry cycle and a given rust layer. The long term behaviour of the modelling is examined in this sub-section.

During the wet stage, the potential is cathodic and the current (determined by oxygen reduction on the rust layer) is weak. When the rust layer begins to dry, the corrosion current increases and the potential becomes more anodic. At the end of the drying, the current dwindles because of the blocking of the anodic sites to finally be nought, whereas the potential goes on increasing (Fig. 14).

This current/potential behaviour qualitatively agrees with those published [7]. If the range of potential in the modelling is slightly larger, the main difference is with the order of magnitude of the maximum current density (about 500–1000 μA/cm^2 measured, compared to about 20 μA/cm^2 in the modelling). This apparent discrepancy is likely due to the fact that the measurements have been made on bare iron,

progressively rusted by wet–dry cycles (with a steady decrease in the maximum current density) whereas the modelling supposes a relatively thick rust layer already present (as expected in condition of long term corrosion). The rust layer of the model corresponds thus to a large number of cycles and lower current density are consistent with the experimental results cited.

During the drying, more anodic potentials allow the re-oxidation of the ferrous species, which regenerates the rust layer in its initial oxidation state and will allow a next cycle to begin (during the next condensation of an electrolyte film) by the reduction of reducible ferric species (γ-FeOOH). It may then be possible to loop the modelling of a wet–dry cycle to assess long term behaviour.

The modelling developed for the different stages of the wet–dry cycle provides reasonable values for the damages. These damages are given by expressions (11) for the reduction of γ-FeOOH during wetting and (24) for oxygen reduction during the wet stage.

These expressions depend on the rust layer properties, like γ-FeOOH fraction β or porosity and tortuosity (ε and τ) and thickness (L, which determines S). As the rust layer contributes to AC phenomena and undergoes many modifications during wet–dry cycle all these properties are likely to evolve with time and thus to modify the corrosion rate. The long term prediction of AC requires then to know how these properties will evolve.

Experimental results presented elsewhere [26,27] suggest that the rust layer mean porosity remains nearly constant with time. In a first approximation, it is considered that tortuosity also remains stable with time.

Composition measurements on ancient rust layers (Fig. 15) allow to establish the evolution of β ratio as a function of rust layer age [26,27]. When taking about 100 c/yr, the interpolation of β evolution as a function of the number of cycles N_c is obtained:

$$\beta = 0.6 \exp\left(-\frac{N_c}{100,000}\right). \tag{34}$$

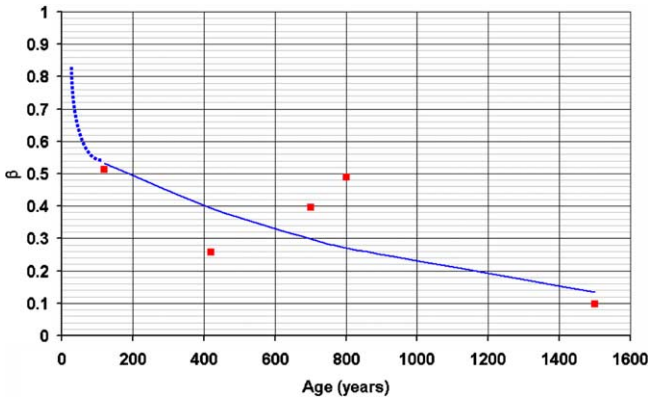

Fig. 15. γ-FeOOH fraction (β) evolution as a function of age (square) and its interpolation (solid line) and during the first years of corrosion (dotted line).

The interpolation (34) was established only in the aim to obtain a value for β, given a certain AC corrosion time, that is considered equivalent to a certain number of wet–dry cycles. Nevertheless, FeOOH transformations may be "thermodynamic", and thus essentially linked to aging time or depending on mechanisms occurring during the wet–dry cycles and thus determined essentially by the number of cycles. It would seem that the difference of crystallographic structure between α- and γ-FeOOH requires a dissolution–precipitation process rather than a direct solid transformation one [11]. The number of wet–dry cycles (and their duration) would then be the β determining factor.

It may be that for younger rust layer (some years old), γ-FeOOH fraction is far higher and that its evolution is faster. The likely initial β evolution is also given in Fig. 15.

The growth of the rust layer thickness after a wet–dry cycle is related to the total damage ($p = p_\gamma + p_O$) during this cycle (amount of dissolved iron). It is considered that all the dissolved iron is converted into FeOOH—in α or γ structure—after the drying. If the rust layer is assumed composed only of α-FeOOH and γ-FeOOH, the thickness variation after a cycle, ΔL is

$$\Delta L = p\frac{M_{\mathrm{FeOOH}}}{\rho(1-\varepsilon)V_{\mathrm{Fe}}} \tag{35}$$

with ρ the mean α-FeOOH and γ-FeOOH density, M_{FeOOH} the FeOOH molar mass, ε the rust layer porosity and V_{Fe} the molar volume of iron.

Using the relations (11) and (24) for the damages during the wetting and wet stages and the relations (34) and (35) for the evolution of the rust layer during the wet–dry cycles, one can obtain the damages after a given number of cycles.

When considering only the damage due to oxygen reduction during a wet stage, the long term damages remain reasonable or even weak (for instance a score of microns for 100 years). However, with the chosen model for the rust layer and the approximations done on the variations of the different parameters with time, the damage due to oxygen reduction during the wet stage depends only on the γ-FeOOH fraction β within the rust layer. In this modelling, the corrosion rate slow down experimentally observed [2] can then come only from a decrease of β. This, indeed, corresponds qualitatively to the measured time evolution of β (Fig. 15).

The calculated damage for γ-FeOOH reduction is largely unrealistic (about 30 cm for 100 years). In this case, the damage is proportional to the γ-FeOOH fraction β and to the rust layer thickness L (indeed proportional to the γ-FeOOH amount). If β does not decrease enough rapidly, the increase of the rust layer thickness leads to a more and more important amount of reducible γ-FeOOH available for reduction during the wetting and thus to a quasi-exponential growth of the damage. The reduction by a factor of 5 observed for γ-FeOOH fraction over about 1000 years is by far too small to balance the increase of the γ-FeOOH amount due to the growth of the rust layer.

To be able to extrapolate the modelling developed for an AC wet–dry cycle to long term periods, corresponding to a large number of cycles, it is necessary to refine the rust layer description. A first refining could be to consider spatial variations of β

inside the rust layer. Indeed the characterisation of the rust has shown that the outer zone of the rust layer is richer in γ-FeOOH than the inner zone. With the growth of the rust layer, a large amount of the γ-FeOOH in the outer zone may then be no longer in contact with the metal and then will be no more reducible The amount of the γ-FeOOH that reduces during each cycle, and thus the damage, is consequently limited. It forces also oxygen to enter deeper into the rust layer before to be in contact with the reduction sites and it increases thus the diffusion path (which lessens the oxygen reduction current).

The measurements [26,27] have exhibited that the porosity of the rust layer remains nearly constant with time. However, local porosity may evolve, for instance with a densification of the inner zones. Corrosion would then lower, both because of the difficulties to remove the corrosion products and because it becomes hard for the γ-FeOOH to reduce in the outer zones (it requires a electric contact with the metal). A parameter that takes into account the connectivity of γ-FeOOH islands could thus be introduced. This parameter would tend to diminish with time and also when going far from the metal/rust interface. It would be related to the percolation notion as the connectivity of the γ-FeOOH islands can be seen as the percolation of a γ-FeOOH paths from the metal until a given distance from the electrolyte/rust interface.

6. Conclusion

A first step in modelling the complex processes occurring during an AC wet–dry cycle is proposed. It is based on mechanistic considerations, so as to provide a more reliable support for long term predictions of AC on iron based nuclear waste containers than empirical extrapolations give. The guiding principle of the modelling is to focus on the different electrochemical reactions associated with the wetting and wet stages of the wet–dry cycle, namely γ-FeOOH and oxygen reduction and anodic sites blocking.

This modelling gives acceptable order of magnitude for the damages and current–potential behaviour description for a given wet–dry cycle. However, it appears still too basic for long term prediction. Indeed, it does not consider the modification of the composition and the structure of the rust layer during the wet–dry cycle which seems to be mainly responsible for the observed AC rate slow down with time. The modelling reveals to be also a fruitful tool for investigating the mechanisms involved in AC.

Moreover, the description of the rust layer, required to establish the modelling, has led to a wide characterisation effort [26,27], which has provided a better knowledge of the rust layers composition and morphology.

To go further in long term AC modelling, it is suggested to focus on rust layer properties evolution as well as electrolyte–rust layer interactions, especially during wetting and drying stages. Moreover, the reduction of oxygen on a rust layer has been thoroughly investigated [7,16]. The modelling developed in this paper focuses however on a ''old'' rust layer and assumes stationary conditions, which is not the

case of the experimental results already published. The validation of the modelling requires then new and specific experiments that will be the subject of future works.

References

[1] M. Pourbaix, The linear bilogarithmic law for atmospheric corrosion, in: W.H. Ailor (Ed.), Atmospheric Corrosion, John Wiley & Sons, New York, 1982, p. 107.
[2] M. Pourbaix, A. Pourbaix, Corrosion 45 (1) (1989) 71.
[3] D. Landolt, Traité des Matériaux: Corrosion et Chimie de Surface des Matériaux, Presse Polytechniques et Universitaires Romandes, Lausanne, 1993.
[4] T.E. Graedel, R.P. Frankenthal, J. Electrochem. Soc. 137 (8) (1990) 2385.
[5] U.R. Evans, C.A.J. Taylor, Corros. Sci. 12 (1972) 227.
[6] M. Stratmann, Corros. Sci. 27 (8) (1987) 869.
[7] M. Stratmann, H. Streckel, Corros. Sci. 30 (6/7) (1990) 681, and 697.
[8] M. Stratmann, K. Bohnenkamp, H.J. Engell, Corros. Sci. 23 (9) (1983) 969.
[9] M. Stratmann, K. Hoffmann, Corros. Sci. 29 (11/12) (1989) 1329.
[10] A. Cox, S.B. Lyon, Corros. Sci. 36 (7) (1994) 1167.
[11] A. Hickling, D.J.G. Ives, Electrochim. Acta 20 (1975) 63.
[12] E.R. Vago, E.J. Calvo, M. Stratmann, Electrochim. Acta 39 (11/12) (1994) 1655.
[13] J.W. Schulze, S. Mohr, M.M. Lohrengel, J. Electroanal. Chem. 154 (1983) 57.
[14] A. Kuch, Corros. Sci. 28 (3) (1988) 221.
[15] S.H. Zhang, S.B. Lyon, Corros. Sci. 35 (1–4) (1993) 713.
[16] M. Stratmann, J. Müller, Corros. Sci. 36 (2) (1994) 327.
[17] A. Nishikata, Y. Ichiara, Y. Hayashi, T. Tsuru, J. Electrochem. Soc. 144 (4) (1997) 1244.
[18] M. Yamashita, H. Nagano, R.A. Oriani, Corros. Sci. 40 (9) (1998) 1447.
[19] V. Jovancicevic, J.O.M. Bockris, J. Electrochem. Soc. 133 (1986) 1797.
[20] E.R. Vago, E.J. Calvo, M. Stratmann, Electrochim. Acta 39 (1994) 1655.
[21] E.R. Vago, E.J. Calvo, J. Electroanal. Chem. 388 (1995) 161.
[22] E.R. Vago, E.J. Calvo, J. Chem. Soc. Faraday. Trans. 91 (15) (1995) 2323.
[23] M. Stratmann, Metalurgia i Odlewnictwo 16 (1) (1990) 45.
[24] M. Stratmann, Berichte der Bunsengesellschaft für Physikalische Chemie 94 (1990) 629.
[25] D. Fyfe, The atmosphere, in: L.L. Shreir, R.A. Jarman, G.T. Burstein (Eds.), Corrosion, vol. 1, third ed., Butterworth–Heinemann, Oxford, 1994, p. 2.
[26] P. Dillmann, V. Vigneau, F. Mazaudier, C. Blanc, S. Hoerlé, EFC Series 36 (2002) 316.
[27] P. Dillmann, M. Mazaudier, S. Hoerlé, Corros. Sci. (2004) in press.
[28] K. Kaneko, K. Inouye, Bull. Chem. Soc. Jpn. 47 (5) (1974) 1139.
[29] T. Misawa, K. Hashimoto, S. Shimodaira, Corros. Sci. 14 (1974) 131.
[30] D.C. Cook, S.J. Oh, R. Balasubramanian, M. Yamashita, Hyperfine Interact. 122 (1–2) (1999) 59.
[31] T. Misawa, T. Kyuno, W. Suëtaka, S. Shimodaira, Corros. Sci. 11 (1971) 35.
[32] M. Stratmann, K. Bohnenkamp, T. Ramchandran, Corros. Sci. 27 (9) (1987) 905.
[33] T. Nishimura, H. Katayama, K. Noda, T. Kodama, Corros. Sci. 42 (2000) 1611.
[34] M. Yamashita, H. Miyuki, Y. Matsuda, H. Nagano, T. Misawa, Corros. Sci. 36 (2) (1994) 283.
[35] T. Kamimura, M. Stratmann, Corros. Sci. 43 (2001) 429.
[36] F. King, M. Kolar, D.W. Shoesmith, Corrosion NACE, paper no. 380, 1996.
[37] M. Baklouti, N. Midoux, F. Mazaudier, D. Feron, J. Hazard. Mat. B 85 (2001) 273.
[38] F. Mazaudier, D. Feron, M. Baklouti, N. Midoux, J. Phys. 11 (2001) 259.
[39] J.-E. Hiller, Werkst. Korros. 17 (11) (1966) 943.
[40] M. Morcillo, S. Feliu, J. Simancas, Br. Corros. J. 28 (1) (1993) 50.
[41] J.H. Wang, F.I. Wei, Y.S. Chang, H.C. Shih, Mater. Chem. Phys. 47 (1) (1997) 1.
[42] M. Stratmann, H. Streckel, K.T. Kim, S. Crockett, Corros. Sci. 30 (6/7) (1990) 715.
[43] T. Misawa, Corros. Sci. 13 (1973) 659.